Huixi Li, Xiaoyan Zhu, Qing Tang, Shengping Wang, and Jingxian Yu
Three-dimensional NiFe layered double hydroxide nanowire/ nanoporous Ni/nickel foam for efficient oxygen evolution
Journal of Electrochemical Society, 2020; 167(14):146513-1-146513-8

3D nanowire NiFe-LDHs/Ni/NF with efficient electrocatalytic performance for water electrolysis

Journal:	*Journal of The Electrochemical Society*
Manuscript ID	JES-101996.R1
Manuscript Type:	Research Paper
Date Submitted by the Author:	27-Aug-2020
Complete List of Authors:	Li , Huixi; China University of Geosciences Wang, Shengping; China University of Geosciences, Faculty of Materials Science and Chemistry Tang, Qing; China University of Geosciences Zhu, Xiaoyan; China University of Geosciences Yu, Jingxian; The University of Adelaide, School of Chemistry and Physics
Keywords:	layered double hydroxide, nickel foam, nanopore, oxygen evolution reaction, electrocatalyst

3D nanowire NiFe-LDHs/Ni/NF with efficient electrocatalytic performance for water electrolysis

Huixi Li [a], Shengping Wang[a, *], Qing Tang[a], Xiaoyan Zhu[a], Jingxian Yu[b, *]

[a] Faculty of Materials Science and Chemistry, China University of Geosciences, Wuhan 430074, China

[b] ARC Centre of Excellence for Nanoscale BioPhotonics (CNBP), School of Chemistry and Physics, The University of Adelaide, Adelaide, SA 5005, Australia

[*] Corresponding Author. spwang@cug.edu.cn (S. Wang), Jingxian.Yu@adelaide.edu.au (J. Yu)

Abstract: NiFe layered double hydroxides (NiFe-LDHs) are considered a promising substitute for noble metal electrocatalysts in the oxygen evolution reaction (OER). In this work, a NiFe-LDH/Ni/NF nanowire electrocatalyst was designed and prepared on nickel foam (NF) by means of a polystyrene (PS) microsphere template and two-step in situ electrodeposition method. The electrocatalysts had a high specific surface area, an increased number of electrocatalytic active sites and an improved electrochemical stability. in the NiFe-LDHs/Ni/NF, the nickel nanoporous interlayer bonded closely with the NF matrix and became loaded with NiFe-LDHs nanowires at the same time, which accelerated the electron transfer of the catalyst nanowires to the matrix, increased the apparent active area, and promoted the OER. As expected, upon achieving a current density of 10 mA cm^{-2}, the NiFe-LDHs/Ni/NF exhibited a lower overpotential of 247 mV, a lower Tafel slope of 35.52 mV dec^{-1} and better durability than those of Ni/NF or NiFe-LDHs/NF. In addition, the overall water splitting system with NiFe-LDHs/Ni/NF as the anode and Ni/NF as the cathode reached a current density of 10 mA cm^{-2} at a low potential of 1.55 V.

Keywords: layered double hydroxide; nickel foam; nanopore; oxygen evolution reaction; electrocatalyst

1. Introduction

The growing demand for energy has led to in-depth research on efficient/low-cost and environmentally friendly sustainable energy production and conversion systems, especially in the area of water splitting [1-3]. Hydrogen, as an ideal clean fuel, has been considered a promising alternative energy to replace traditional fossil fuels in the future. Electrocatalytic water splitting is an ideal method for hydrogen fuel production, but it is limited by the slow kinetics of the oxygen evolution reaction (OER), which causes a severe overpotential demand [4-8]. Therefore, it is imperative to explore efficient electrocatalysts for the OER. In recent years, transition metal layered double hydroxide (LDH) electrocatalysts have been widely studied by researchers for their easy-to-control composition, unique electronic structure [9-10], high OER electrocatalytic efficiency and anti-corrosion stability during the OER in alkaline conditions and much lower price than RuO_2 and IrO_2-based noble metal electrocatalysts [11-13]. Among a variety of LDH electrocatalysts, NiFe-LDHs showed the best OER electrocatalytic performance under alkaline conditions [14], and their turnover frequency was much higher than that of IrO_2 [15]. However, the low electronic conductivity inhibits the practical application of this catalyst as an electrode material [16-17].

To overcome this disadvantage, many researchers combined LDH electrocatalysts with conductive materials (such as nickel foams (NFs), copper foams, and carbon fiber cloths) to construct three-dimensional (3D) high-efficiency OER electrocatalysts [18-22]. The 3D structural materials with good conductivity can provide a large specific surface area to increase the contact area between the electrocatalyst and the electrolyte, accelerate the electron transport in the reaction process and increase the active sites of the electrocatalytic reaction [23]. However, it is still unable to meet the demand for a low OER overpotential. Ren and co-workers used an electrochemical redox method to form copper nanowires in situ on copper foam and loaded it with LDH electrocatalysts [20, 24], which further improved the conductivity and surface active area of the electrocatalyst, thus significantly improving its OER performance. Jin and coworkers used a template method combined with an electrodeposition method to prepare a nanoarray nickel-supported NiCo-LDH electrocatalyst on conductive glass [25], which greatly improved the OER electrocatalytic performance. The in situ introduction of a metal interlayer can improve the electrocatalytic ability of the LDH electrocatalysts.

In light of the above analysis, this study employs a PS microsphere template combined with a two-step electrodeposition method to prepare nanoporous nickel-based NiFe-LDH nanowire electrocatalysts on a NF matrix [26]. A NF matrix enables the fabrication of a 3D electrocatalyst and improves the conductivity of the electrocatalyst, while the introduction of a nickel nanoporous interlayer can further improve the conductivity of the electrocatalyst and increase the apparent activity area of the electrocatalyst. The experimental results show that, compared with those for Ni/NF and NiFe-LDHs/NF, the prepared NiFe-LDHs/Ni/NF electrocatalyst shows the best OER electrocatalytic performance. The electrocatalyst only needs a low overpotential of 247 mV at 10

mA cm^{-2}, and exhibits an extremely low Tafel slope of 35.52 mV dec^{-1} and good electrocatalytic stability.

2. Preparation of the electrocatalysts

2.1 Electrocatalyst preparation

The NiFe-LDHs/Ni/NF was prepared by the polystyrene (PS) sphere template method and two-step in situ electrodeposition method, and the specific preparation process was as follows.

2.1.1 Synthesis of PS/NF electrode

The NF (1 cm × 2 cm, 1.6 mm thickness, 0.42 g cm^{-3} density) was ultrasonically treated in a 5 M HCl solution for 30 min to remove the surface NiO_x layer. Then, the NF was washed with deionized water and anhydrous ethanol 3 times and dried in a vacuum drying box. Using the pretreated NF as the substrate, the PS sphere template was prepared by a vertical deposition self-assembly technique. The average size of the PS microspheres was 500 nm, and the mass fraction was 2.5%.

The PS microsphere suspension and ethanol were mixed at a volume ratio of 4:3. The mixture was then slowly dripped onto the surface of deionized water. Due to the surface tension of the water, a monolayer PS microsphere film formed on the liquid surface. To closely align the PS microspheres, a small amount of surfactant containing sodium dodecyl sulfate (0.1% by mass fraction) was injected onto the liquid surface. The NF substrate was inserted vertically into the deionized water for 20 s, and then it was lifted slowly to ensure that the PS microspheres were uniformly dispersed on it. Finally, tightly arranged single-layer PS templates were obtained. The prepared PS templates were collected and dried at 90 ℃ for 0.5 h to obtain the PS/NF.

2.1.2 Synthesis of the Ni/NF electrode

The Ni layer was deposited on the PS/NF with an electrolyte containing 20 mM $NiSO_4$ and 40 mM NH_4Cl (pH = 6.0) by cathodic electrodeposition with a 1 cm × 1 cm nickel plate as the anode. The current density was 0.5 mA cm^{-2}, and the electrodeposition times were 10, 20, 30, and 40 min. Then, the electrodes were washed with deionized water and anhydrous ethanol 3 times and dried in a vacuum drying box. Then, the PS spheres embedded in the Ni film were dissolved by trichloromethane, and Ni/NF with Ni nanopores was obtained. The Ni nanopore size was related to the size of the PS microspheres.

2.1.3 Synthesis of the NiFe-LDHs/Ni/NF electrode

The electrode samples were synthesized by electrodeposition in a three-electrode system at 25 ℃ with platinum as the counter electrode, a saturated calomel electrode (SCE) as the reference electrode and the Ni/NF material as the work electrode. The electrolyte was composed of 3 mM $Ni(NO_3)_2$ $6H_2O$ and 3 mM $Fe(NO_3)_3$ $9H_2O$. The electrodeposition was carried out at -1.0 V (vs. SCE) constant voltage, and the deposition times were 30, 60, 150, 300, and 600 s. After deposition,

the electrode was removed from the electrolyte, washed with deionized water and anhydrous ethanol 3 times, and dried in a vacuum drying box.

2.2 Physical characterization

The morphology and composition of the samples were determined by scanning electron microscopy (SEM, Hitachi-S4800) and energy dispersive X-ray spectrometry (EDX) on the same scanning electron microscope. The crystallinity of the product was characterized by X-ray diffraction (XRD, Bruker/D8-FOCUS) on a powder diffractometer that used Cu Kα (λ = 1.5418 Å) radiation at a scanning rate of 10 °min^{-1} between 10 °and 90 °.

2.3 Electrochemical measurements

All electrochemical measurements were carried out at 25 ℃ using a CHI 660D electrochemical workstation with the three-electrode system. The abovementioned electrodes (Ni/NF, NiFe-LDHs/NF and NiFe-LDHs/Ni/NF) with dimensions of 1 cm ×1 cm were used as the work electrode, a saturated calomel electrode was the reference electrode, a platinum plate electrode was the auxiliary electrode and freshly prepared oxygen-saturated 1 M KOH solution was the electrolyte. All the potentials measured were converted to reversible hydrogen standard potential (RHE) using Eq. 1.

$$E_{RHE}\,(V) = E_{SCE} + 0.0591pH + E^{0}_{SCE} = E_{SCE} + 0.0591pH + 0.231 \quad (1)$$

Electrochemical impedance spectroscopy (EIS) was performed by the AC impedance technique in 1 M KOH at 1.58 V (η = ~350 mV) from 100 mHz to 100 kHz with an AC voltage of 5 mV. The scanning range for cyclic voltammetry (CV) was 1.2-1.3 V, and the scanning rates were 10, 20, 30, 40, 50 mV s^{-1}. The scanning range for the anodic polarization curve was 1.2-1.8 V, and the scanning rate was 5 mV s^{-1}.

To obtain the apparent activation energy (E_a) of the OER, linear sweep voltammetry (LSV) curves at various temperatures (30-50 ℃) were also measured. The scanning rate for the hydrogen evolution and overall water splitting polarization curves was also 5 mV s^{-1}.

The stability of the electrocatalyst was measured with chronopotentiometric (CP) curves with a current density of 10 mA cm^{-2} for 24 h. At the same time, the stability of the catalyst was measured by a polarization curve before and after 5000 cycles of CV from 1.2-1.6 V. All LSV polarization curves were recorded after activation by a CP scan with a constant current density until a stable state was reached. All the polarization curves were corrected by eliminating the iR drop with respect to the ohmic resistance of the solution. The SCE was used to measure the potential of the RHE with the Pt electrode in a H_2 atmosphere, thus calibrating the SCE.

3. Results and discussion

3.1 Optimization of the deposition time

The LSV and EIS curves for optimization of the deposition time of the nickel nanoporous interlayer in NiFe-LDHs/Ni/NF and the deposition time of the NiFe-LDHs nanosheet on the composite catalyst are shown in Fig. 1. When the nickel nanoporous interlayer deposition time was 20 min and the surface NiFe-LDH nanosheet deposition time was 300 s, the prepared composite electrocatalyst had the lowest OER overpotential and charge transfer resistance (R_{ct}). Therefore, the composite electrocatalysts prepared under these conditions were selected for physical and electrochemical characterization.

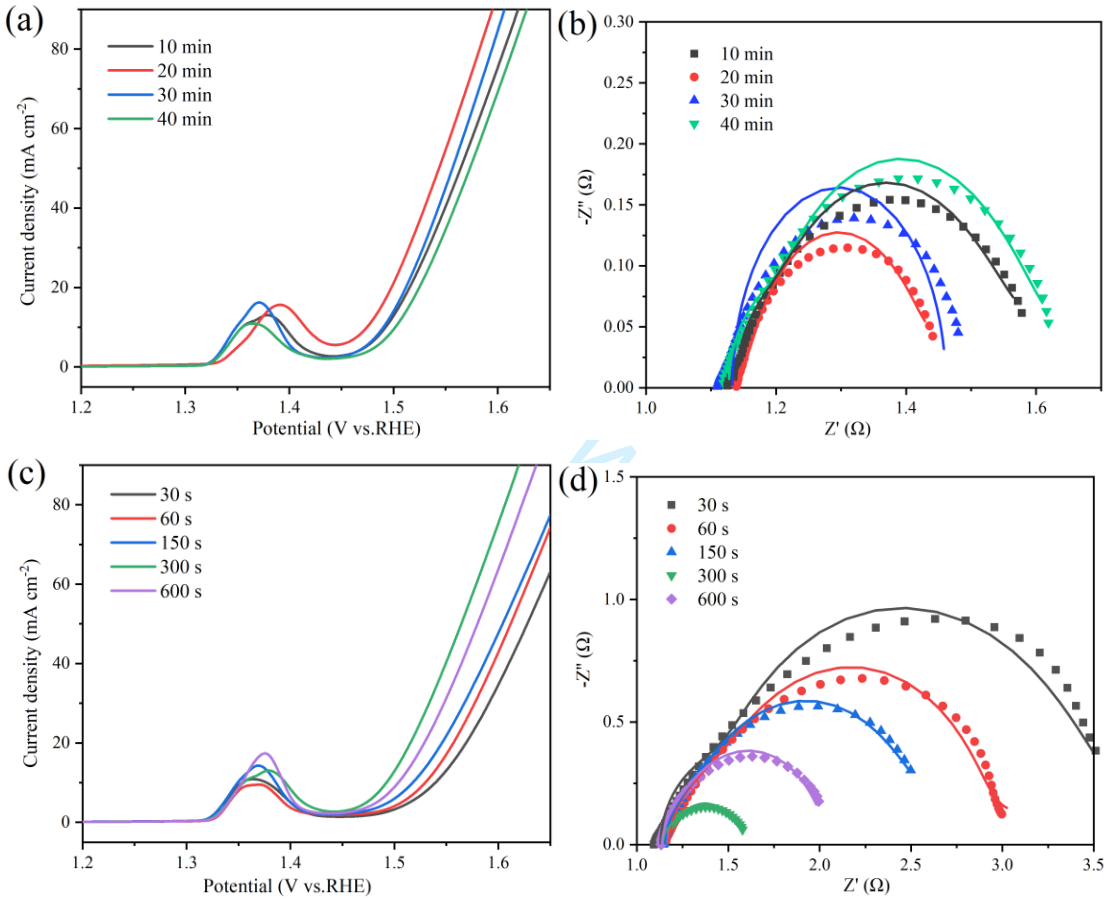

Fig. 1 LSV and EIS curves for the optimization of the nickel nanoporous interlayer deposition time in the NiFe-LDHs/Ni/NF (a, b) and deposition time of the NiFe-LDHs nanowires (c, d).

3.2 SEM and XRD

In the experimental section, the preparation processes for several electrocatalysts are described in detail. In this paper, the SEM was used to analyze the effect of the introduction of a nickel nanoporous interlayer on the structure and morphology of the electrocatalyst. The SEM images of

the electrocatalysts are shown in Fig. 2. The diameter and depth of the nickel nanopores were ~500 nm and ~100 nm, respectively. The NiFe-LDHs/NF were stacked in two-dimensional nanowires, and the NiFe-LDHs/Ni/NF still retained the nanowire structure, but the nanowires were uniformly dispersed. Due to the introduction of the nickel nanoporous interlayer, the conductivity of the NF matrix and the contact surface with the electrolyte increased so that NiFe hydroxide was deposited quickly and uniformly on the matrix. In the literature, LDH electrocatalysts prepared by electrodeposition are amorphous.

In addition, the EDX elemental mapping analysis (Fig. 2d) indicated that the Ni, Fe, and O elements were homogeneously distributed across the entire NiFe-LDHs/Ni/NF sample. The XRD spectras of the Ni/NF, NiFe-LDHs/NF and NiFe-LDHs/Ni/NF catalysts are shown in Fig. 2e. The strong peaks at 44.5 °, 51.8 ° and 76.4 ° are the diffraction peaks from the base Ni, and no new diffraction peaks appeared, indicating that the LDH electrocatalysts deposited on NF were amorphous [18, 27].

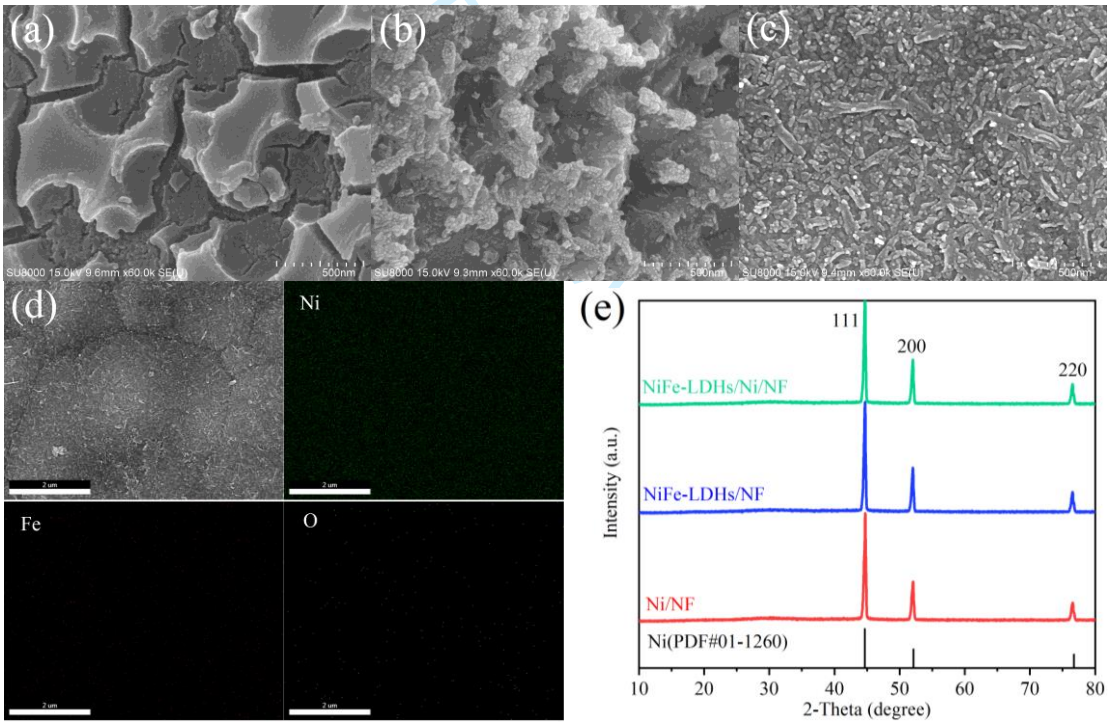

Fig. 2 SEM images of Ni/NF (a), NiFe-LDHs/NF (b) and NiFe-LDHs/Ni/NF (c), and EDX (d), XRD (e) spectras of NiFe-LDHs/Ni/NF.

3.3 Polarization curve (overpotential (η), exchange current density (j^0), and Tafel slope (b), E_a)

To measure the catalytic performance of the oxygen evolution of the electrocatalysts, anodic polarization curves were obtained. Fig. 3a shows the anodic polarization curves of the various electrocatalysts in 1 M KOH modified by iR_s (i is Faraday current, and R_s is uncompensated

electrolyte resistance). The η-log$i$ curves for the oxygen evolution overpotential η and logarithmic current density (log$i$) fitted by the Tafel formula are shown in Fig. 3b. The slope and potential intercept of each curve are calculated and analyzed by origin 8.6, and the results are shown in Table 1.

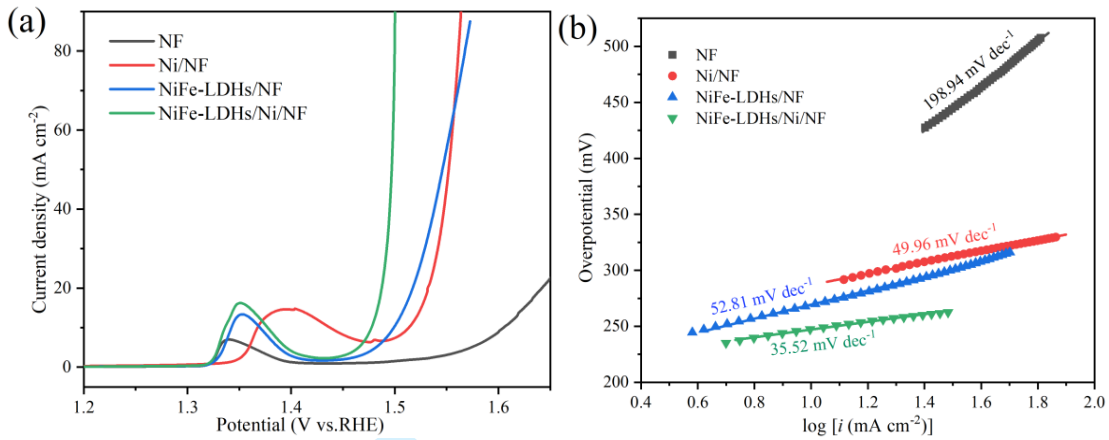

Fig. 3 Polarization curves corrected by iR_s (a) and Tafel fitting curves (b) of the samples.

Table 1 Kinetic fitting parameters of the polarization curves (b, η_{10}, and j^0), equivalent circuits (R_s, C_f, R_f, Q_{dl}, n, R_{ct}, and Chi-squared) of the samples and the activation energy (E_a) and electric double layer capacitance (C_{dl}) values.

	NF	Ni/NF	NiFe-LDHs/NF	NiFe-LDHs/Ni/NF
b (mV dec^{-1})	198.94	49.96	52.81	35.52
η_{10} (mV)	375	279	269	247
j^0 (A cm^{-2})	9.510×10^{-5}	4.373×10^{-4}	1.077×10^{-3}	1.631×10^{-3}
E_a (kJ mol^{-1})	-	36.08	30.29	27.94
C_{dl} (mF cm^{-2})	-	10.94	12.46	14.95
R_s (Ω cm^{-2})	1.184	1.143	1.208	1.135
C_f (F cm^{-2})	0.02082	0.04191	0.05641	0.03895
R_f (Ω cm^{-2})	11.61	0.01147	1.123	0.02173
Q_{dl} (S s^n cm^{-2})	0.04479	0.07215	0.07909	0.1786
n	0.6829	0.6813	0.6198	0.8756
R_{ct} (Ω cm^{-2})	2.063	1.536	0.9337	0.3558
Chi-squared	3.896×10^{-4}	5.976×10^{-5}	2.691×10^{-4}	2.551×10^{-5}

In Fig. 3a, each polarization curve showed an oxidation peak at approximately 1.38 V, corresponding to the oxidation process of Ni hydroxide (i.e., $Ni(OH)_2 \rightarrow NiOOH$), after which, NiOOH formed by oxidation catalyzed water oxidation. The oxygen evolution mechanism of the Ni-based LDH electrocatalysts in alkaline solution can be expressed as follows [10].

The preconversion of $Ni(OH)_2$ is:

$$Ni(OH)_2 + OH^- \leftrightarrow NiOOH + H_2O + e^- \quad (2)$$

NiOOH electrocatalyzes the specific reaction process of the OER as follows:

$$NiOOH + OH^- \leftrightarrow NiO(OH)_2 + e^- \quad (3)$$

$$NiO(OH)_2 + OH^- \leftrightarrow NiOO(OH) + H_2O + e^- \quad (4)$$

$$NiOO(OH) + OH^- \leftrightarrow NiOO(OH)_2 + e^- \quad (5)$$

$$NiOO(OH)_2 + OH^- \leftrightarrow NiOO_2(OH)^- + H_2O \quad (6)$$

$$NiOO_2(OH)^- \leftrightarrow NiOOH + O_2 + e^- \quad (7)$$

The overpotential η of the OER is one of the important indexes to judge the difficulty of the anodic reaction. The overpotential η_{10} corresponding to a current density of 10 mA cm^{-2} is calculated to compare the electrocatalytic performance of each electrocatalyst for oxygen evolution. The overpotential η_{10} of the NiFe-LDHs/Ni/NF obtained by introducing a nickel nanoporous interlayer was only 247 mV, which is smaller than that of the NiFe-LDHs/NF of 269 mV and even better than that of commercial IrO_2 and RuO_2 electrocatalysts. At the same time, the NiFe-LDHs/Ni/NF had a very low Tafel slope of 35.52 mV dec^{-1}, showing a high electrocatalytic performance, indicating that the introduction of a nickel nanoporous interlayer improved the electrocatalytic performance of the LDH electrocatalysts for the OER. This is mainly because the introduction of the nickel nanoporous interlayer increased the conductivity of the electrocatalyst; it increased the contact area between the electrocatalyst and the electrolyte, thus accelerating the mass transfer and charge transfer processes.

The Tafel fitting curves of the LDH electrocatalyst are shown in Fig. 3b. The Tafel slope *b* can characterize the change in the overpotential with current density. The smaller slope *b* is the slower overpotential changes with the current density, and the better catalytic performance of the electrocatalyst [28]. At the same time, the control steps in the process of oxygen evolution can be

judged according to the b value. Takanabe et al. [29] discussed the correlation between the Tafel slope and rate determination steps based on microdynamic analysis. In theory, when the surface species formed in the step prior to the rate determination step are dominant, the Tafel slope is 120 mV dec^{-1}, while in other cases, the Tafel slope should be less than 120 mV dec^{-1}. When Eqs. 4 or 6 is used as the rate determination step, a Tafel slope of 30 mV dec^{-1} should be observed, and the vacancy coverage should be high. If the rate determination step is Eq. 7, the Tafel slope is approximately 40 mV dec^{-1}. In this study, since the Tafel slope of the NiFe-LDHs/Ni/NF was 35.52 mV dec^{-1}, Eq. 7 was used as the rate determining step.

According to electrochemical theory, the exchange current density can characterize the polarization of the electrode and the reversibility of the electrode reaction [30]. It is generally believed that a high exchange current density means that the electrode is difficult to polarize and has good reversibility, and the electrode reaction easily occurs. As shown in Table 1, the NiFe-LDHs/Ni/NF with the introduction of a nickel nanoporous interlayer had the highest exchange current density herein of 1.631 $\times 10^{-3}$ mA cm^{-2}, which is better than that of the NiFe-LDHs/NF and indicated good electrocatalytic activity for oxygen evolution. This may be because the introduction of nickel nanopores increased the overall conductivity of the catalyst and increased the electrocatalytic activity exposure area of the electrocatalyst, thus increasing the OER activity of the NiFe-LDHs/Ni/NF.

The E_a characterizes the degree of difficulty of a reaction. Reducing the E_a of a reaction is a common feature of all catalytic reactions. The smaller E_a is the better catalytic performance of the electrode, and the easier chemical reaction. By plotting the anodic polarization curve at various temperatures (T), E_a can be determined using the Arrhenius law by Eq. 8 [31-32].

$$\ln i = \ln A - \frac{E_a}{RT} \quad (8)$$

where A is the pre-exponential factor, R is the gas constant (8.314 mol^{-1} K^{-1}), T is the absolute temperature, and E_a is the molar activation energy.

The anodic polarization curves at various temperatures (30-50 ℃) of the Ni/NF, NiFe-LDHs/NF and NiFe-LDHs/Ni/NF are shown in Fig. 4. In the oxygen evolution zone, the current density corresponding to the oxygen evolution potential of 1.58 V (η = 350 mV) was selected as i, and ln$i$-1/T was linearly fitted (as shown in Fig. 4b). The E_a value was determined by the slope.

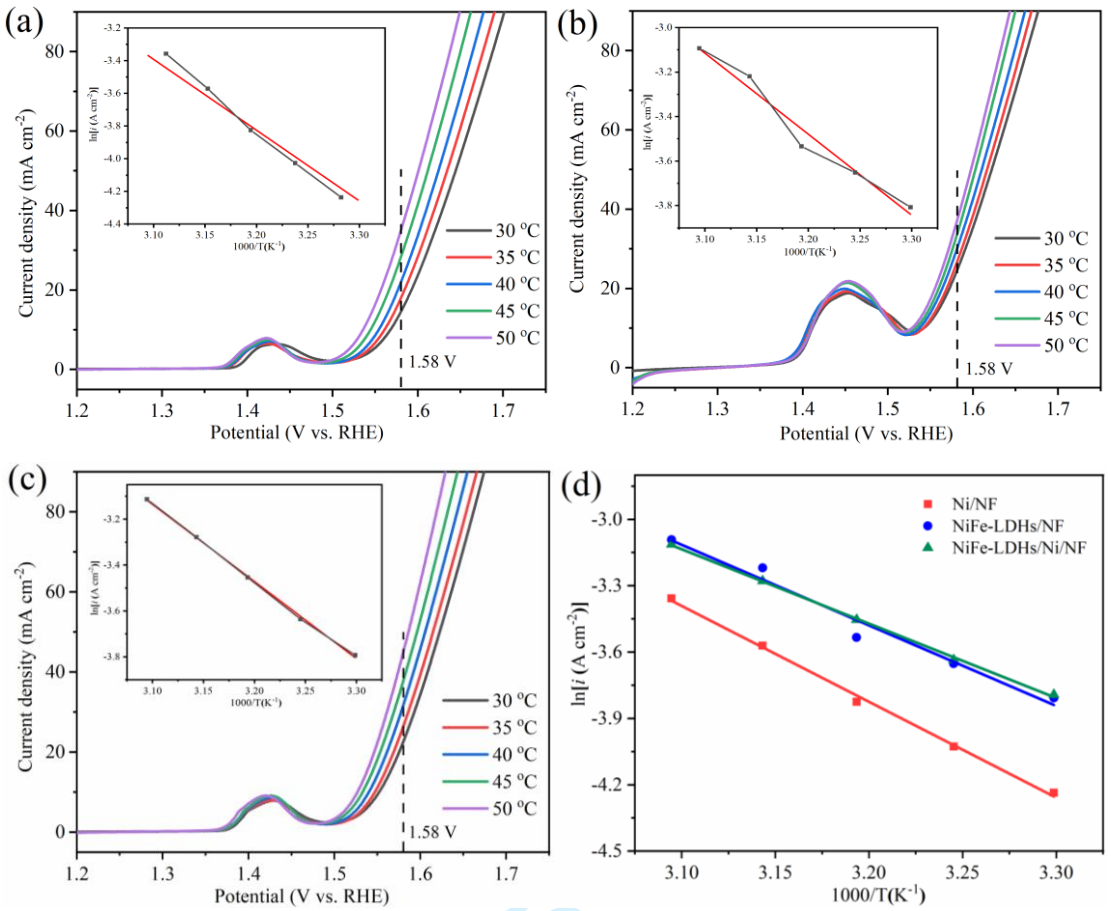

Fig. 4 Polarization curves and ln*i*-1/*T* fitting curves of Ni/NF (a), NiFe-LDHs/NF (b) and NiFe-LDHs/Ni/NF (c) at various temperatures, and their ln*i*-1/*T* fitting curves (d).

There is an obvious relationship between E_a and the oxygen evolution reaction, and a low E_a enables the anodic oxygen evolution reaction. The Arrhenius linear curve ln*i*-1/*T* of various electrocatalysts is shown in Fig. 4d. The slopes correspond to the oxygen evolution activity of various electrocatalysts in this electrochemical process, and the corresponding E_a data are listed in Table 1. At 1.58 V, the E_a of the Ni/NF was 36.08 kJ mol^{-1}, which indicates poor oxygen evolution performance. The OER E_a of the NiFe-LDHs/NF was 30.29 kJ mol^{-1} lower than that of the Ni/NF, while the E_a of the NiFe-LDHs/Ni/NF with a nickel nanoporous interlayer decreased to 27.94 kJ mol^{-1}, and the electrocatalytic performance of the OER was obviously improved. The main reason was that the introduction of a nickel nanoporous interlayer increased the conductivity of the electrocatalyst electrode, accelerated the electron transfer between the matrix and the catalyst, and promoted the transformation of the active site from Ni^{2+} to Ni^{3+}, which as a stronger catalytic activity; that is, the transformation of $Ni(OH)_2 \rightarrow NiOOH$ promoted the conversion of $Fe(OH)_3 \rightarrow FeOOH$ and reduced the energy barrier of the OER. The NiFe-LDH nanowires formed by electrodeposition on the surface of the electrode substrate were also scattered and stacked, which increased the interface area between the electrocatalyst and the electrolyte.

3.4 Double layer capacitance (C_{dl})

A large number of studies have shown that the apparent electrochemical active area is proportional to the number of catalytic active points in the OER, and C_{dl} values can be used to evaluate the apparent electrochemical active area [33-35]. To further study the effect of the introduction of a nickel nanoporous interlayer on the active points of the OER on the electrode surface, a narrow C_{dl} potential region was selected, and CV was carried out at various scanning rates. The narrow potential from 1.2 V to 1.3 V was selected, in which only the non-Faraday charging process occurred. All voltammetry curves were recorded between 1.2 V and 1.3 V as a function of the scan rate, v ($5 \leq v \leq 100$ mV s^{-1}), and of the current measured, i_E, at constant potential (1.25 V). C_{dl} was obtained by the slope of the fitting curve i_E vs. v. Figs. 5a-c show the CV curves of Ni/NF, NiFe-LDHs/NF and NiFe-LDHs/Ni/NF at various scanning rates in the double layer range (1.2-1.3 V), and Fig. 5d shows the i_E vs. v fitting curves of the electrocatalysts.

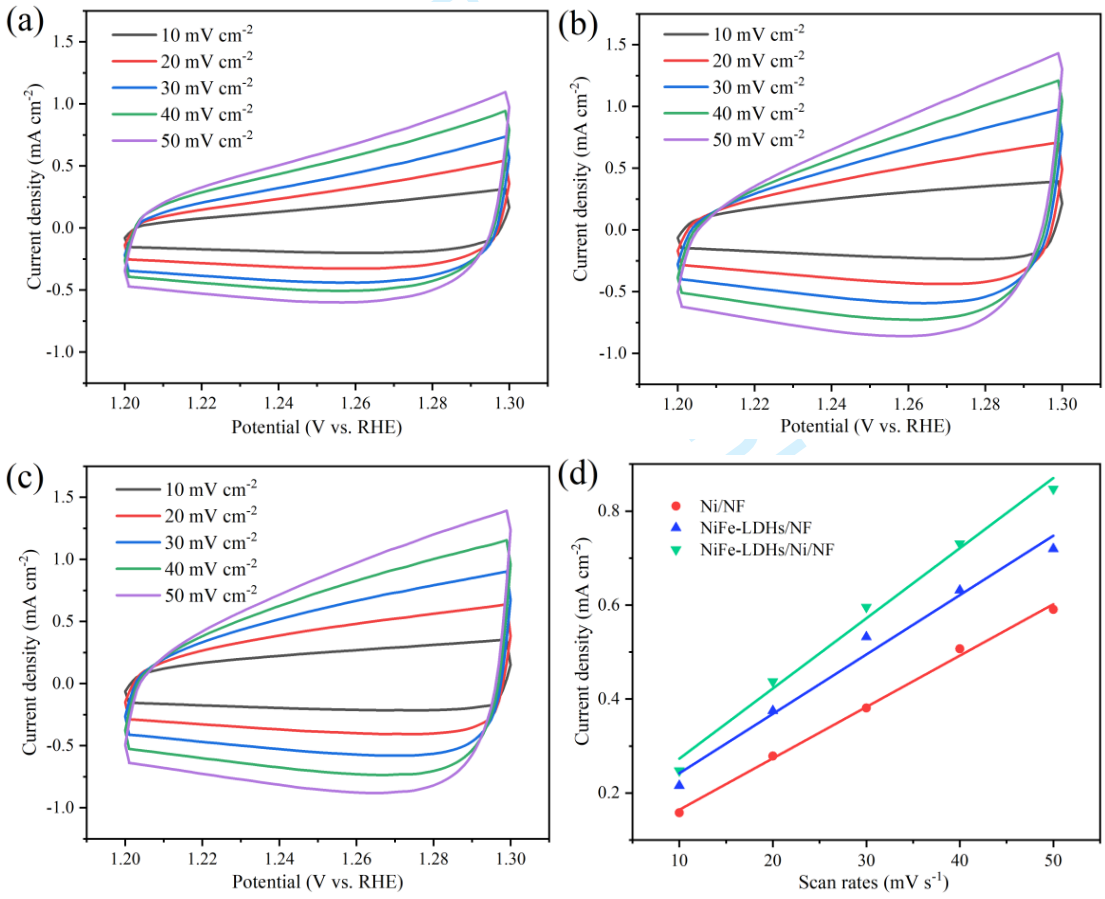

Fig. 5 CV curves of Ni/NF (a), NiFe-LDHs/NF (b) and NiFe-LDHs/Ni/NF (c) with various scanning rates over the potential range of 1.2-1.3 V, and their fitting curves for a current density of constant potential (1.25 V) as a function of the scanning rate (d).

The C_{dl} values of the electrocatalysts are listed in Table 1. Before the introduction of the nickel nanoporous interlayer, the C_{dl} of the NiFe-LDH was 12.46 mF cm^{-2}. After the introduction, the C_{dl} of the NiFe-LDHs/Ni/NF increased to 14.95 mF cm^{-2}, which is 2.49 mF cm^{-2} higher than that of the NiFe-LDHs. The results show that the NiFe-LDHs/Ni/NF obtained by introducing a nickel nanoporous interlayer had more active sites and a better electrocatalytic activity for oxygen evolution. This was due to the introduction of the nickel nanoporous interlayer, which made the electrocatalyst on the electrode surface form an uneven nanowire stacking structure, which increased the surface area and the number of active sites of the electrocatalyst.

3.5 EIS (R_{ct} and electric double layer capacitance (Q_{dl}))

Employing EIS to study the gas evolution reaction on the surface of a solid electrode is very informative. This paper used this method to study the effect of the nickel nanoporous interlayer on the OER of a NiFe-LDH electrocatalyst. Fig. 6 shows the Nyquist diagram of various catalyst electrodes at 1.58 V (η = 350 mV) in 1 M KOH. It is obvious that there are two capacitive arcs in the whole frequency region of the Nyquist diagram, corresponding to two time constants. The capacitive arc in the middle- and high-frequency regions of the Nyquist complex plan was related to the physical response of the pore structure on the electrocatalyst surface, while the semicapacitive arc in the low-frequency region characterized the electrochemical reaction process between the hydroxide coating and the solution interface of the electrocatalyst.

The equivalent circuit can be represented by R_s (R_fC_f) ($R_{ct}C_{dl}$), and its equivalent circuit diagram is shown in the illustration in Fig. 6. In previous literature reports, this equivalent circuit was commonly applied to fit the impedance data of an electrocatalyst during OER [32, 36-37]. In the equivalent circuit, R_s is the uncompensated solution resistance, R_f is the interface impedance formed by the migration of reactive ions to the electrocatalyst interface layer, and C_f is the capacitance. The (R_fC_f) combination in parallel characterizes the physical response of the electrocatalyst interface in the middle- and high-frequency regions. R_{ct} is the charge transfer resistance of the electrochemical reaction process, and C_{dl} is the corresponding capacitance. The ($R_{ct}C_{dl}$) combination in parallel corresponds to the OER process in the low-frequency region. Considering the nonhomogeneity of the electrode surface, a constant phase element (CPE) is employed instead of a capacitive element (C_{dl}), and the impedance of the CPE can be represented with Eq. 9 [38]:

$$Z_{\mathrm{CPE}} = \frac{1}{Q(jw)^{\mathrm{n}}} \tag{9}$$

where Q is the CPE constant, n is the corresponding dispersion coefficient, and w is the angular frequency.

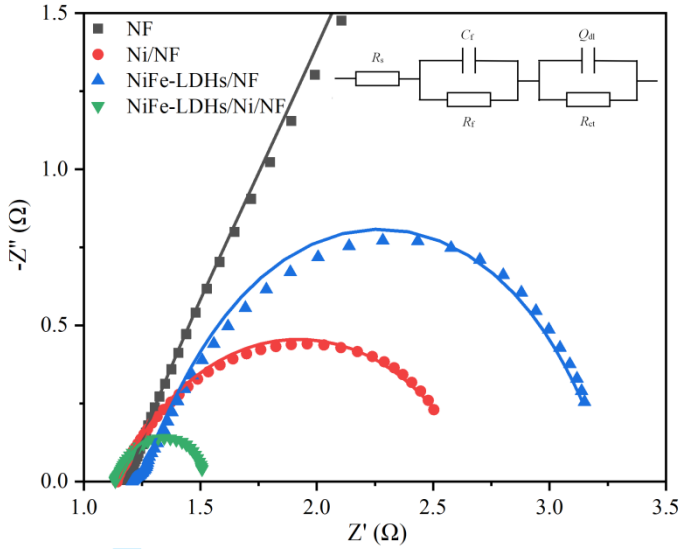

Fig. 6 Nyquist diagrams and corresponding equivalent circuit diagrams of the electrocatalysts.

The chi-squared values of the fitting degree parameters obtained by using the above equivalent circuit were all less than 10^{-3}, indicating that the selected equivalent circuit can well reflect the OER behavior of the electrocatalyst in 1 M KOH. The fitted EIS data for all electrical parameters are listed in Table 1. It can be clearly seen that R_s changed little, suggesting the good stability of the electrolysis system. Several studies have shown that Q_{dl} and R_{ct} can be employed to evaluate and explain the electrocatalytic activity of oxidation/hydroxide electrodes [39]. Large Q_{dl} and low R_{ct} values are considered to be favorable for the occurrence of the oxygen evolution electrocatalytic reaction, suggesting an improved electrocatalytic activity of the electrocatalyst [27]. The R_{ct} of the NiFe-LDHs/Ni/NF in the low-frequency region had the minimum value, and the corresponding Q_{dl} had the maximum value, indicating that the electrocatalyst had the best OER electrocatalytic performance. It can be seen from the data in Table 1 that the C_f of the Ni/NF decreased obviously and had a minimum value after the NF surface became coated with the nickel nanoporous layer, but the R_{ct} of the OER reaction did not change much, and the corresponding Q_{dl} increased obviously, indicating that the nickel nanoporous interlayer increased the conductivity and electrocatalytic activity area of the electrode. The NiFe-LDHs/NF had a large coating resistance, small R_{ct} and large Q_{dl}, suggesting that it had poor conductivity but good OER electrocatalytic performance. When the nickel nanoporous interlayer was introduced into the NiFe-LDHs/NF, the C_f of the NiFe-LDHs/Ni/NF decreased sharply, its R_{ct} for the OER decreased obviously, and the corresponding Q_{dl} increased sharply, indicating that the introduction of the nickel nanoporous interlayer can not only increase the conductivity of the NiFe-LDHs but also increase the electrochemical activity area of the electrocatalyst, thus greatly improving the OER performance of the electrocatalyst.

3.6 OER stability test

To evaluate the electrocatalytic stability of the electrocatalysts for the OER, the CP curves of Ni/NF, NiFe-LDHs/NF and NiFe-LDHs/Ni/NF were measured at 10 mA cm^{-2} for 24 h (Fig. 7a). At

first, the potential increased rapidly and then remained stable after reaching a potential plateau region. The potential rise was mainly due to an activation process from $Ni(OH)_2$ to NiOOH on the surface. The stability test curves of the NiFe-LDHs/NF and NiFe-LDHs/Ni/NF showed a stable overpotential plateau in 24 h, indicating that the two electrocatalysts had relatively stable electrocatalytic performance in alkaline solution, while the NiFe-LDHs/Ni/NF showed the lowest overpotential plateau, indicating that the electrocatalyst had the best electrocatalytic performance for oxygen evolution. To test the stability of the NiFe-LDHs/Ni/NF after a long cycle, 5000 voltammetry cycles were performed in the range of 1.2-1.6 V. The polarization curves before and after 5000 cycles were compared. Fig. 7b shows that there was almost no obvious change in the polarization curve before and after the cycle test, and the electrocatalyst still retained an intact nanowire structure after the cycling (as shown in the inset of Fig. 7b), showing that the NiFe-LDHs/Ni/NF had good electrocatalytic stability.

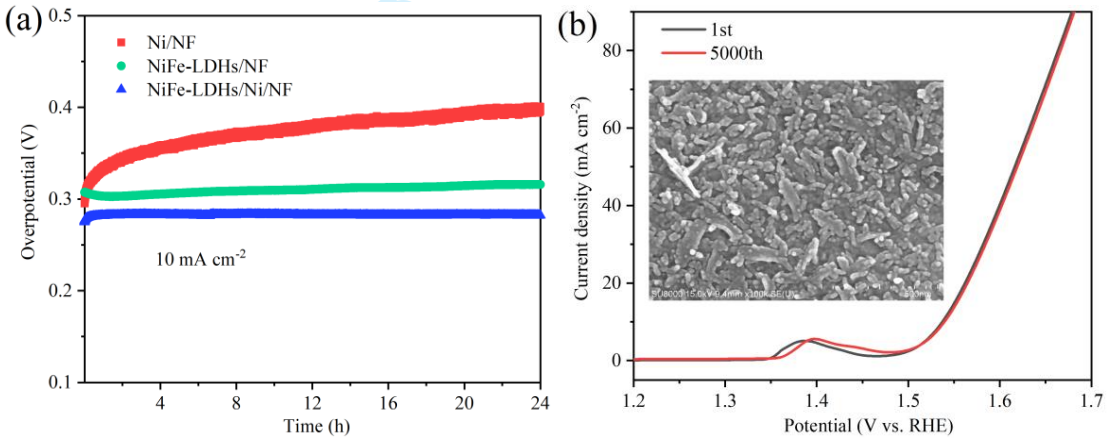

Fig. 7 The CP curves of the samples at 10 mA cm^{-2} for 24 h (a) and polarization curves of the NiFe-LDHs/Ni/NF before and after 5000 cycles from 1.2-1.6 V (b), where the inset is an SEM image of the NiFe-LDHs/Ni/NF surface after the cyclic stability test.

3.7 HER and overall water splitting (OWS)

Considering that nanostructured metals show good hydrogen evolution performance, HER performance tests of the Ni/NF, NiFe-LDHs/NF and NiFe-LDHs/Ni/NF were performed. It can be clearly seen that the nickel nanoporous layer supported by Ni/NF shows good HER electrocatalytic performance (Fig. 8a), and its overpotential at the current density of 10 mA cm^{-2} was only 52 mV. At the same time, the NiFe-LDHs/Ni/NF was employed as the anode, and the Ni/NF was used as the cathode to assemble an overall water splitting system to measure the LSV curve (Fig. 8b). Only 1.55 V overpotential was needed to reach 10 mA cm^{-2}, showing a good overall water splitting performance. The NiFe-LDHs/Ni/NF is a good OER electrocatalyst, and the Ni/NF is a good HER electrocatalyst.

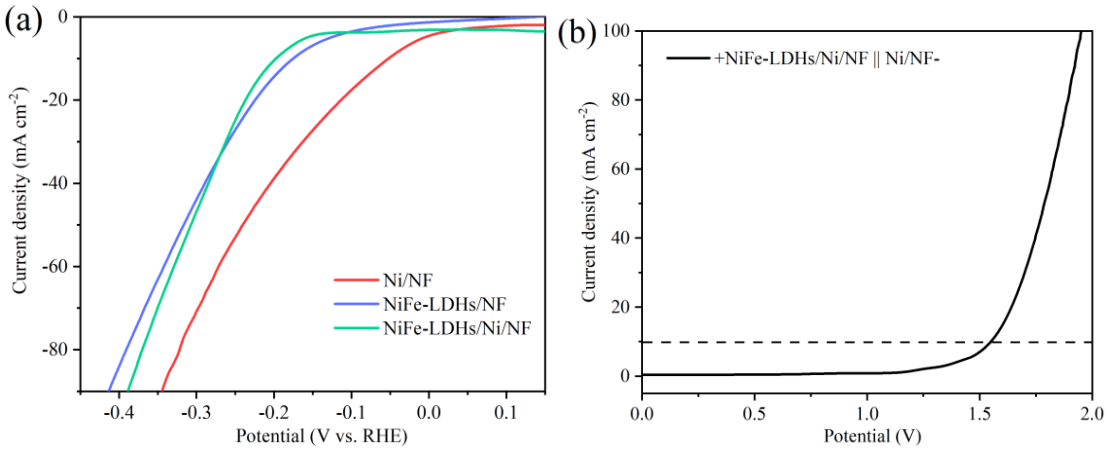

Fig. 8 Hydrogen evolution polarization curves (a) and overall water splitting polarization curves (b) with the NiFe-LDHs/Ni/NF as the anode and the Ni/NF as the cathode.

4. Conclusion

In short, 3D nanowire electrocatalysts based on binary Ni-Fe hydroxides were prepared by a simple electrodeposition method and used as efficient OER electrocatalysts. By using a relatively high surface area, an enhanced electron transport and a synergistic effect, the well-designed 3D NiFe-LDHs/Ni/NF nanowire electrode shows efficient OER electrocatalytic activity. It had a small oxygen evolution overpotential of 247 mV at a current density of 10 mA cm^{-2} and a low Tafel slope of 35.52 mV dec^{-1}, and it also had good durability in alkaline media. The overall water splitting device of the electrochemical system was tested, and only a 1.55 V overpotential was needed to reach a 10 mA cm^{-2} current density. This is a simple and feasible method for manufacturing efficient LDH electrocatalysts and provides new insight for the development of effective OER electrocatalysts.

References

[1] P. Wang, Y. Lin, L. Wan, B. Wang, Construction of a janus MnO_2-NiFe electrode via selective electrodeposition strategy as a high-performance bifunctional electrocatalyst for rechargeable zinc-air batteries, *ACS Appl. Mater. Interfaces*, 2019, 11, 37701-37707. https://doi.org/10.1021/acsami.9b12232

[2] C. Ye, M. -Q. Wang, S. -J. Bao, C. Ye, Micropore-boosted layered double hydroxide catalysts: EIS analysis in structure and activity for effective oxygen evolution reactions, *ACS Appl. Mater. Interfaces*, 2019, 11, 30887-30893. https://doi.org/10.1021/acsami.9b09144

[3] L. Xu, L. Cao, W. Xu, Z. Pei, One-step electrosynthesis of NiFe-NF electrodes for highly efficient overall water splitting, *Appl. Surf. Sci.*, 2020, 503, 144122 https://doi.org/10.1016/j.apsusc.2019.144122

[4] Z. Wang, S. Zeng, W. Liu, X. Wang, Q. Li, Z. Zhao, F. Geng, Coupling molecularly ultrathin sheets of NiFe-layered double hydroxide on $NiCo_2O_4$ nanowire arrays for highly efficient overall water-splitting activity, *ACS Appl. Mater. Interfaces*, 2017, 9, 1488-1495. https://doi.org/10.1021/acsami.6b13075

[5] G. Zhang, Y. -S. Feng, W. -T. Lu, D. He, C. -Y. Wang, Y. -K. Li, X. -Y. Wang, F. -F. Cao, Enhanced catalysis of electrochemical overall water splitting in alkaline media by Fe doping in Ni_3S_2 nanosheet arrays, *ACS Catal.*, 2018, 8, 5431-5441. https://doi.org/10.1021/acscatal.8b00413

[6] H. Liang, A. N. Gandi, C. Xia, M. N. Hedhili, D. H. Anjum, U. Schwingenschlögl, H. N. Alshareef, Amorphous NiFe-OH/NiFeP electrocatalyst fabricated at low temperature for water oxidation applications, *ACS Energy Lett.*, 2017, 2, 1035-1042. https://doi.org/10.1021/acsenergylett.7b00206

[7] M. Qian, S. Cui, D. Jiang, L. Zhang, P. Du, Highly efficient and stable water-oxidation electrocatalysis with a very low overpotential using FeNiP substitutional-solid-solution nanoplate arrays, *Adv. Mater.*, 2017, 29, 1704075. https://doi.org/10.1002/adma.201704075

[8] C. Zhang, J. Zhao, L. Zhou, Z. Li, M. Shao, M. Wei, Layer-by-layer assembly of exfoliated layered double hydroxide nanosheets for enhanced electrochemical oxidation of water, *J. Mater. Chem. A*, 2016, 4, 11516-11523. https://doi.org/10.1039/c6ta02537d

[9] Y. Wang, M. Qiao, Y. Li, S. Wang, Tuning surface electronic configuration of NiFe LDHs nanosheets by introducing cation vacancies (Fe or Ni) as highly efficient electrocatalysts for oxygen evolution reaction, *Small*, 2018, 14, 1800136. https://doi.org/10.1002/smll.201800136

[10] X. Li, X. Hao, Z. Wang, A. Abudula, G. Guan, In-situ intercalation of NiFe LDH materials: an efficient approach to improve electrocatalytic activity and stability for water splitting, *J. Power Sources*, 2017, 347, 193-200. https://doi.org/10.1016/j.jpowsour.2017.02.062

[11] Z. Lu, L. Qian, Y. Tian, Y. Li, X. Sun, X. Duan, Ternary NiFeMn layered double hydroxides as highly-efficient oxygen evolution catalysts, *Chem. Commun.*, 2016, 52, 908-911. https://doi.org/10.1039/c5cc08845c

[12] L. Qian, Z. Lu, T. Xu, X. Wu, Y. Tian, Y. Li, Z. Huo, X. Sun, X. Duan, Trinary layered double hydroxides as high-performance bifunctional materials for oxygen electrocatalysis, *Adv. Energy Mater.*, 2015, 5, 1500245. https://doi.org/10.1002/aenm.201500245

[13] Z. Yang, J. -Y. Zhang, Z. Liu, Z. Li, L. Lv, X. Ao, Y. Tian, Y. Zhang, J. Jiang, C. Wang, "Cuju"-structured iron diselenide-derived oxide: a highly efficient electrocatalyst for water oxidation, *ACS Appl. Mater. Interfaces*, 2017, 9, 40351-40359. https://doi.org/10.1021/acsami.7b14072

[14] Z. Cai, L. Li, Y. Zhang, Z. Yang, J. Yang, Y. Guo, L. Guo, Amorphous nanocages of Cu-Ni-Fe hydr(oxy)oxide prepared by photocorrosion for highly efficient oxygen evolution, *Angew. Chem. Int. Ed.*, 2019, 58, 4189-4194. https://doi.org/10.1002/anie.201812601

[15] L. Trotochaud, S. L. Young, J. K. Ranney, S. W. Boettcher, Nickel-iron oxyhydroxide oxygen-evolution electrocatalysts: the role of intentional and incidental iron incorporation, *J. Am. Chem. Soc.*, 2014, 136, 6744-6753. https://doi.org/10.1021/ja502379c

[16] H. Liu, Y. Wang, X. Lu, Y. Hu, G. Zhu, R. Chen, L. Ma, H. Zhu, Z. Tie, J. Liu, Z. Jin, The effects of Al substitution and partial dissolution on ultrathin NiFeAl trinary layered double hydroxide nanosheets for oxygen evolution reaction in alkaline solution, *Nano Energy*, 2017, 35, 350-357. https://doi.org/10.1016/j.nanoen.2017.04.011

[17] S. Dutta, A. Indra, Y. Feng, T. Song, U. Paik, Self-supported nickel iron layered double hydroxide-nickel selenide electrocatalyst for superior water splitting activity, *ACS Appl. Mater. Interfaces*, 2017, 9, 33766-33774. https://doi.org/10.1021/acsami.7b07984

[18] X. Lu, C. Zhao, Electrodeposition of hierarchically structured three-dimensional nickel-iron electrodes for efficient oxygen evolution at high current densities, *Nat. Commun.*, 2015, 6, 6616. https://doi.org/10.1038/ncomms7616

[19] T. Zhang, L. Hang, Y. Sun, D. Men, X. Li, L. Wen, X. Lyu, Y. Li, Hierarchical hetero-Ni3Se4@NiFe LDH micro/nanosheets as efficient bifunctional electrocatalysts with superior stability for overall water splitting, *Nanoscale Horiz.*, 2019, 4, 1132-1138. https://doi.org/10.1039/c9nh00177h

[20] L. Yu, H. Zhou, J. Sun, F. Qin, F. Yu, J. Bao, Y. Yu, S. Chen, Z. Ren, Cu nanowires shelled with NiFe layered double hydroxide nanosheets as bifunctional electrocatalysts for overall water splitting, *Energy Environ. Sci.*, 2017, 10, 1820-1827. https://doi.org/10.1039/c7ee01571b

[21] P. Babar, A. Lokhande, H. H. Shin, B. Pawar, M. G. Gang, S. Pawar, J. H. Kim, Cobalt iron hydroxide as a precious metal-free bifunctional electrocatalyst for efficient overall water splitting, *Small*, 2018, 14, 1702568. https://doi.org/10.1002/smll.201702568

[22] A. -L. Wang, H. Xu, G. -R. Li, NiCoFe layered triple hydroxides with porous structures as high-performance electrocatalysts for overall water splitting, *ACS Energy Lett.*, 2016, 1, 445-453. https://doi.org/10.1021/acsenergylett.6b00219

[23] J. Ji, L. Zhang, H. Ji, Y. Li, X. Zhao, X. Bai, X. Fan, F. Zhang, R. S. Ruoff, Nanoporous $Ni(OH)_2$ thin film on 3D ultrathin-graphite foam for asymmetric supercapacitor, *ACS Nano*, 2013, 7, 6237-6243. https://doi.org/10.1021/nn4021955

[24] L. Yu, H. Zhou, J. Sun, F. Qin, D. Luo, L. Xie, F. Yu, J. Bao, Y. Li, Y. Yu, S. Chen, Z. Ren, Hierarchical Cu@CoFe layered double hydroxide core-shell nanoarchitectures as bifunctional electrocatalysts for efficient overall water splitting, *Nano Energy*, 2017, 41, 327-336. https://doi.org/10.1016/j.nanoen.2017.09.045

[25] Z. Zhao, H. Wu, H. He, X. Xu, Y. Jin, A high-performance binary Ni-Co hydroxide-based water oxidation electrode with three-dimensional coaxial nanotube array structure, *Adv. Funct. Mater.*, 2014, 24, 4698-4705. https://doi.org/10.1002/adfm.201400118

[26] L. Gui, Z. Chen, Y. Song, W. Zhu, Q. Yu, D. Wu, T. Zheng, Preparation and electrocatalytic performance of nanosphere array PbO_2 electrode on stainless steel-based grid-like ZnO film, *J. Electrochem. Soc.*, 2019, 166, 12. https://doi.org/10.1149/2.1231912jes

[27] H. Li, L. Zhang, S. Wang, J. Yu, Accelerated oxygen evolution kinetics on NiFeAl-layered double hydroxide electrocatalysts with defect sites prepared by electrodeposition, *Int. J. Hydrogen*

Energ., 2019, 44, 28556-28565. https://doi.org/10.1016/j.ijhydene.2019.09.155

[28] Y. Wang, D. Yan, S. E. Hankari, Y. Zou, S. Wang, Recent progress on layered double hydroxides and their derivatives for electrocatalytic water splitting, *Adv. Sci.*, 2018, 5, 1800064. https://doi.org/10.1002/advs.201800064

[29] T. Shinagawa, A. T. Garcia-Esparza, K. Takanabe, Insight on Tafel slopes from a microkinetic analysis of aqueous electrocatalysis for energy conversion, *Sci. Rep.*, 2015, 5, 13801. https://doi.org/10.1038/srep13801

[30] H. Yang, B. Chen, H. Liu, Z. Guo, Y. Zhang, X. Li, R. Xu, Effects of manganese nitrate concentration on the performance of an aluminum substrate β-PbO_2-MnO_2-WC-ZrO_2 composite electrode material, *Int. J. Hydrogen Energ.*, 2014, 39, 3087-3099. https://doi.org/10.1016/j.ijhydene.2013.12.091

[31] L. Hui, Y. Xue, B. Huang, H. Yu, C. Zhang, D. Zhang, D. Jia, Y. Zhao, Y. Li, H. Liu, Y. Li, Overall water splitting by graphdiyne-exfoliated and -sandwiched layered double-hydroxide nanosheet arrays, *Nat. Commun.*, 2018, 9, 5309. https://doi.org/10.1038/s41467-018-07790-x

[32] H. Li, Z. Chen, Q. Yu, W. Zhu, W. Cui, Effects of tungsten carbide on the electrocatalytic activity of PbO_2-WC composite inert anodes during zinc electrowinning, *J. Electrochem. Soc.*, 2017, 164 , 14. https://doi.org/10.1149/2.0791714jes

[33] P. Zhang, L. Li, D. Nordlund, H. Chen, L. Fan, B. Zhang, X. Sheng, Q. Daniel, L. Sun, Dendritic core-shell nickel-iron-copper metal/metal oxide electrode for efficient electrocatalytic water oxidation, *Nat. Commun.*, 2018, 9, 381. https://doi.org/10.1038/s41467-017-02429-9

[34] H. Liang, L. Li, F. Meng, L. Dang, J. Zhuo, A. Forticaux, Z. Wang, S. Jin, Porous two-dimensional nanosheets converted from layered double hydroxides and their applications in electrocatalytic water splitting, *Chem. Mater.*, 2015, 27, 5702-5711. https://doi.org/10.1021/acs.chemmater.5b02177

[35] Y. Liu, Y. Bai, Y. Han, Z. Yu, S. Zhang, G. Wang, J. Wei, Q. Wu, K. Sun, Self-supported hierarchical FeCoNi-LTH/$NiCo_2O_4$/CC electrodes with enhanced bifunctional performance for efficient overall water splitting, *ACS Appl. Mater. Interfaces*, 2017, 9, 36917-36926. https://doi.org/10.1021/acsami.7b12474

[36] X. -L.Zhou, Z. -G.Ye, X. -Z. Hua, A. -H. Zou, Y. -H. Dong, Electrocatalytic activity and stability of Ti/IrO_2 + MnO_2 anode in 0.5 M NaCl solution, *J. Solid State Electro*, 2010, 14, 1213-1219. https://doi.org/10.1007/s10008-009-0966-3

[37] Y. -Y. Hou, J. -M. Hu, L. Liu, J. -Q. Zhang, C. -N. Cao, Effect of calcination temperature on electrocatalytic activities of Ti/IrO_2 electrodes in methanol aqueous solutions, *Electrochim. Acta*, 2006, 51, 6258-6267. https://doi.org/10.1016/j.electacta.2006.04.008

[38] Y. Lai, Y. Li, L. Jiang, W. Xu, X. Lv, J. Li, Y. Liu, Electrochemical behaviors of co-deposited Pb/Pb–MnO_2 composite anode in sulfuric acid solution-Tafel and EIS investigations, *J. Electroanal. Chem.*, 2012, 671, 16-23. https://doi.org/10.1016/j.jelechem.2012.02.011

[39] Z. -G.Ye, H. -M. Meng, D. -B. Sun, Electrochemical impedance spectroscopic (EIS)

investigation of the oxygen evolution reaction mechanism of Ti/IrO_2+MnO_2 electrodes in 0.5 M H_2SO_4 solution, *J. Electroanal. Chem.*, 2008, 621, 49-54. https://doi.org/10.1016/j.jelechem.2008.04.009